https://doi.org/10.1016/j.jobe.2023.107371

Response surface modeling and optimization scheme of an internally cooled liquid desiccant air conditioning system

Yanling Zhang*[a,b], Hao Zhang[a], Hongxing Yang[b], Yi Chen*[c], Chun Wah Leung[a]

a. School of Professional Education and Executive Development, The Hong Kong Polytechnic University, Hong Kong, China

b. Renewable Energy Research Group, Department of Building Environment and Energy Engineering, The Hong Kong Polytechnic University, Hong Kong, China

c. College of Marine Equipment and Mechanical Engineering, Jimei University, Xiamen, China

Highlights

An internally cooled liquid desiccant air conditioning system is proposed.

An optimal strategy combining RSM and DFA for the system is presented.

Two-factor effects of operational parameters on system performance are investigated.

Propose monthly optimization operating schemes for Hong Kong environments.

The optimized scheme outperforms cooling capacity by 23.7% over the previous plan.

Abstract

The application of an internally cooled liquid desiccant air conditioning system ($LDAC$) is a promising energy-saving and emission-reduction scheme for hot and humid areas like Hong Kong. A combined system consists of a liquid desiccant dehumidification (LDD) and a regenerative indirect evaporative cooling ($RIEC$) can operate without a power-intensive compressor. It can handle the cooling and dehumidification requirements of various seasons independently. The internally cooled LDD initially removes the latent heat from hot and humid air before it is cooled by the $RIEC$. To ensure efficient energy utilization, the cooling capacity of the exhaust air is captured by the LDD to assist in the dehumidification and initial cooling of the fresh air, which alleviates the efficiency deterioration of the desiccant. An all-fresh air system is used for better indoor air quality. For a system with many influencing parameters, the response surface method (RSM) and multi-objective optimization are used to optimize and

* Corresponding authors: chenyi0511@jmu.edu.cn (Y Chen); yanling.zhang@connect.polyu.hk (Y Zhang)

assess the potential and performance of the system. The validated response surface model is used to optimize six critical environmental and operational parameters. The system cooling capacity (C), latent heat removal rate (Q_d), and dehumidification efficiency (η_d) are used as the optimization objectives. The results show that the system could be used at low airspeed (1.5m/s) and high desiccant concentration (40%) during months with high humidity, which can improve the dehumidification performance of the optimized system by 7.6%. By increasing the extraction ratio of the $RIEC$ by 20% in warmer months, the peak cooling capacity increases by 31.6%. The proposed system can facilitate the application of IEC and LDD technologies and optimize the monthly operation pattern of the system in hot and humid regions.

Keywords: Liquid desiccant dehumidification, Indirect evaporative cooling, Response surface method, System optimization

Nomenclatures

Symbols

A	Heat and mass transfer surface area per unit plate height	(m^2/m)
A_h	PHE height	m
A_w	PHE side length	m
C	cooling capacity	kW
c_p	specific heat at constant pressure	(kJ/kg·K）
d	desirability function	
D	desirability value	
H	channel height	m
h	specific enthalpy	(kJ/kg)
K	heat transfer coefficient	(W/m^2·K)
l	channel length	m
L	minimum response	
m	mass flow rate	(kg/s)
n	Number of desirability functions	
NTU	Number of transfer units	

Q	heat exchange	(kW/m)
Q_d	latent heat removal rate	kW
r	weight	
r_w	Latent heat of vaporization	(kJ/kg)
R^2	coefficients of determination	
RCD	secondary to primary air mass flow ratio in LDD	
re	secondary to primary air mass flow ratio in RIEC	
RH	relative humidity	%
T	maximum response	
t	temperature	(°C)
v	velocity	(m/s)
w	humidity ratio	(kg/kg)
x	x coordinate (fresh air flow direction)	
x_s	solution concentration	(%)
y	y coordinate (water flow direction)	
η_d	dehumidification efficiency	

Greek symbols

α	convection heat transfer coefficient	($W/m^2 \cdot K$)
α_m	mass transfer coefficient	(kg/m2·s)
η	dehumidification efficiency	%
ρ	density	(kg/m^3)

Subscripts

a	air
es	saturation
ew	water and air interface
g	water vapor
in	inlet
lat	latent
out	outlet

s	solution
sen	sensitive
w	water

Abbreviation

LDD	liquid desiccant dehumidification
RIEC	regenerative indirect evaporative cooling
AC	air conditioning
RSM	response surface method
DFA	desirability function approach
CCD	central composite design
ICLDAC	internally cooled liquid desiccant air conditioning system
ANOVA	analysis of variance

1. Introduction

Air conditioning systems are predicted to be the second-largest source of electricity consumption in the next three decades[1]. The energy used by air conditioning (AC) systems makes up between 30 and 50 percent of the annual energy consumption of buildings, especially in hot, humid places like Hong Kong[2, 3]. The energy coefficient of performance (COP) of traditional air-conditioning systems is limited to about 6, and the coupling of the cooling and dehumidification processes leads to a waste energy problem. Condensate is also prone to bacterial growth [4], which is detrimental to indoor air quality. This phenomenon point to the need to use energy-efficient AC systems for hot and humid areas like Hong Kong. Indirect evaporative cooling (IEC) and liquid desiccant dehumidification (LDD) technologies are safe and efficient alternatives to traditional mechanical AC systems in hot and humid regions. This paper presents the results of an investigation to combine these two technologies for energy recovery of air-conditioning systems.

The liquid desiccant can effectively absorb the moisture in the air with a bioaerosol removal rate of 87.3% [5], which is considered a promising method for air conditioning systems to

maintain high air quality with sufficient dehumidification capability. Internal cooling LDD is a viable strategy to increase the vapor pressure difference and keep dehumidification performance while using liquid desiccant for dehumidification in hot and humid regions [6, 7]. Nevertheless, powerful cooling equipment is still necessary due to the high sensible heat load. Combining LDD with regenerative indirect evaporative cooling ($RIEC$), which uses cooled and dried air returned internally to a secondary channel for re-evaporative cooling, provides better system cooling capacity. This internally cooled liquid desiccant air conditioning system ($ICLDAC$) will be a promising energy-saving solution for fresh air treatment to break the regional limitations of IEC and LDD. This system widely applies to various climate regions by taking advantage of decoupling treatment of cooling and dehumidification.

Previous studies on $LDD-IEC$ [8-10] have amply demonstrated excellent energy efficiency and cooling effectiveness performance. Nevertheless, many previous auxiliary cooling methods were based on LDD-added cooling coil systems [10] or performing pre-cooling [8]. Very few were based on IEC facilited internal cooling. A desiccant-enhanced evaporative cooler was proposed by Kozubal et al. [11] which combined LDD and IEC technologies into a single facility to solve the problem of heat and humidity removal in AC systems. Subsequently, a numerical model [12] and a predictive model [13] were established to optimize the desiccant-enhanced evaporative cooler. In these studies, the M-cycle addressed the source of the IEC working airflow, and outdoor air was used as the working air for the LDD. Heat recovery was performed by mixing fresh air and return air to ensure the efficient operation of the system. Table 1 summarizes the characteristics of the three forms of the system. Previously proposed systems are mainly all-fresh air systems [10, 14] (Figure 1-a) or heat recovery systems with mixed exhaust air and fresh air [15] (Figure 1-b). Reapplying exhaust air to the system can improve energy performance [16]. However, this procedure raises the risk of disease transmission in air-conditioned spaces [17, 18]. Few studies have used exhaust air as the internal cooling media in an LDD for all-fresh air systems (Figure 1-c). In this study, The indoor exhaust air will be fully utilized by the proposed fresh air system as the air source for the cooling channel inside the LDD. The plate heat exchanger (PHE) separates dehumidification and working channels. The heat exchange between the two channels ensures low vapor pressure on

the liquid desiccant surface and improves the dehumidification effect. Therefore, the system aims to provide sufficient fresh air intake and utilize exhaust air indirectly without impairing the energy performance.

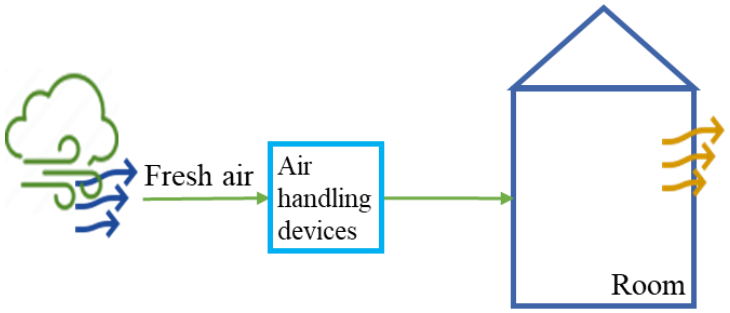

(a) Fresh air ventilation system (existing system)

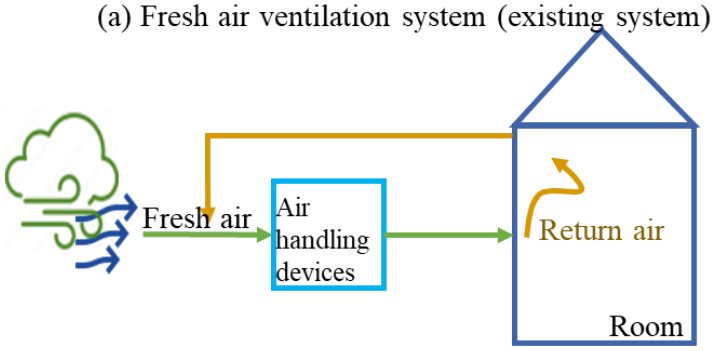

(b) Ventilation system with heat recovery (existing system)

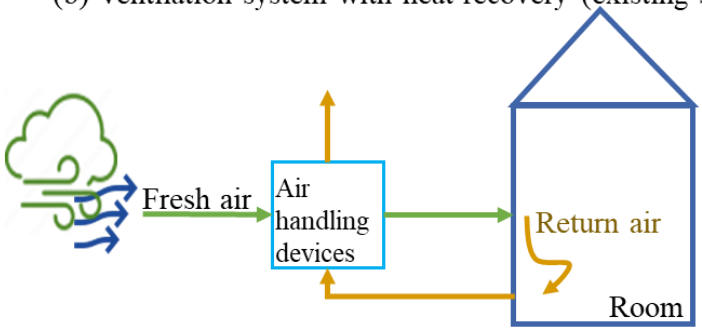

(c) Ventilation system with indirect heat recovery (present system)

Figure 1 Three types of ventilation for the air conditioning system

Table 1 The characteristics of the three ventilation forms of the air conditioning system

System	Disease transmission risk	Dehumidification ability	Exhaust air used?
Fig.1(a)	Low	Low	No
Fig.1(b)	High	Middle	Yes. For heat recovery.
Fig.1(c)	Low	High	Yes. For heat recovery.

For complex systems that integrate fresh air cooling, dehumidification, and exhaust air energy

recovery, parameter analysis [19, 20] and multi-objective optimization are very important to improve system performance. Ren et al. [21] proposed an optimization strategy for complex systems with desiccant wheels and IEC using a multilayer perceptron neural network. Sohani et al. [22] carried out dynamic and static multi-objective optimization on the life cycle and comfort of $LDAC$. Chen et al. [23] addressed the seven most influential parameters in IEC and LDD by sensitivity analysis. Woods and kozubal [24] applied the Monte Carlo method to conduct sensitivity analysis on the design parameters of internally cooled LDD and gave the parameter optimization range. It is required to decide on the optimal values of the elements and explore their interactions once the range of critical factors has been targeted. Response surface method (RSM), assessing the interaction of different variables on response and reducing the number of trials simultaneously, has been widely used in the optimization process. To find the best design with manageable computational costs, Ren et al. [20] employed RSM to optimize the life cycle assessment of cooling and heating systems. An analysis of a liquid dehumidification and regeneration system by Liu et al. [25] used RSM models and genetic algorithms to optimize the dehumidification capacity while maximizing regeneration performance. An experimental-based RSM investigation was carried out by Zhou et al. [26] conducted an experimental RSM study to investigate the variables influencing the capacity to remove the moisture of a solution dehumidification system. Previous studies have amply demonstrated the promise of RSM in multi-factor optimization. However, few studies have used the RSM to optimize the $IEC-LDD$ system. Applying the response surface model might have the potential to identify dominant items and propose optimal regulation strategies in different inlet air conditions.

This study aims to explore the cooling and dehumidifying performance of the $ICLDAC$ system and develop an optimization strategy. The strategy will be based on a response surface method and use the desirability function approach (DFA) further to optimize the design and operational parameters of the system. The newly proposed system fully uses indoor exhaust air as an air source for internal cooling. The total cooling capacity (C), latent heat removal rate (Q_d), and dehumidification efficiency (η_d) are used as the optimization objectives. The influence of six factors, including environmental parameters: temperature (t_{a1}), relative humidity (RH_{a1}),

operational parameters: inlet air velocity (v_{a1}), the concentration of the desiccant (x_s), secondary to primary air ratio in LDD (RCD), and design parameter: number of transfer units of the plate heat exchanger (NTU) on the system performance was also investigated. A case study is presented using the derived models and desirability function for regional applicability analysis in Hong Kong. The results can facilitate the operation and design of internally cooled evaporative cooling dehumidification systems.

2. Proposed system and modeling

2.1.Description of the ICLDAC system

The conceptual diagram of the proposed $ICLDAC$ is shown in Figure 2. Latent heat was initially removed from the fresh air first and achieved initial cooling by internally cooled LDD. A portion of the low-temperature dry fresh air cooled by RIEC is taken as the working air in the $RIEC$ secondary channel, and the remaining air is supplied indoors. After treating the heat and humid load in the room, all the exhaust air is provided to the LDD secondary channels for internal cooling.

A hexagonal heat exchanger is proposed in the internally cooled LDD model to achieve an efficient heat exchange process. The details of establishing the hexagonal internally cooled LDD model [7] are briefly introduced below. The LDD is mathematically modeled as dehumidifying channels and internal cooling channels. The device involves four streams of fluid: fresh air (a_1) and desiccant solution in the dehumidifying channels, and working air (a_5) and water in the cooling channel. The internal cooling channels of LDD indirectly exchange sensible heat and suppress the temperature rise of the solution to ensure the dehumidification capacity. Lithium chloride ($LiCl$) was used as the desiccant in the system modeling. In the IEC mathematical model, the dehumidified and pre-cooled primary air (a_2) from the LDD is indirectly cooled in the IEC. The air supplied to the room handles the heat and moisture load and is reapplied to the LDD as the inlet air of the internal cooling channel.

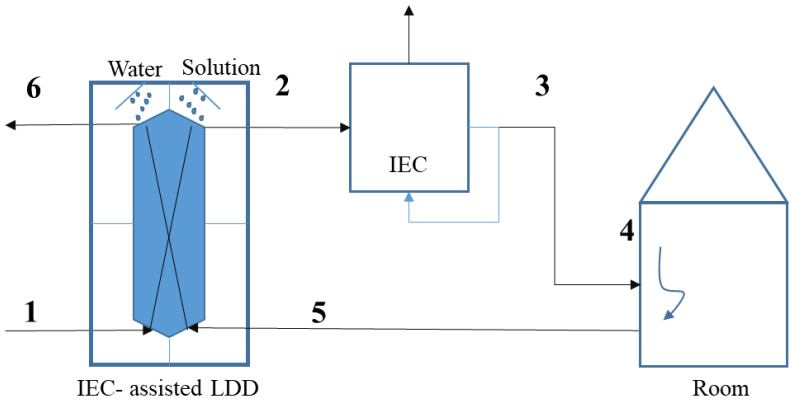

1	Inlet air of LDD	t_{a1}, w_{a1}
2	Outlet air of LDD	t_{a2}, w_{a2}
3	Outlet air of RIEC	t_{a3}, w_{a3}
4	Supply air	t_{a4}, w_{a4}
5	Indoor exhaust air supplied to LDD	t_{a5}, w_{a5}
6	Outlet secondary air for LDD	t_{a6}, w_{a6}
7	Inlet secondary air of IEC	t_{a7}, w_{a7}

Figure 2 Schematic diagram of the ICLDAC system

2.2.Modeling of the *ICLDAC* system

The model for each system component was developed independently. The flowchart for the system model is displayed in Figure 3. The following presumptions are made when modeling the overall system: 1) No heat exchange with the environment and no air leakage in the system unit. 2) Water has constant thermal properties. 3) Mass and heat are only transmitted vertically through the surfaces. 4) The Lewis number is consistent.

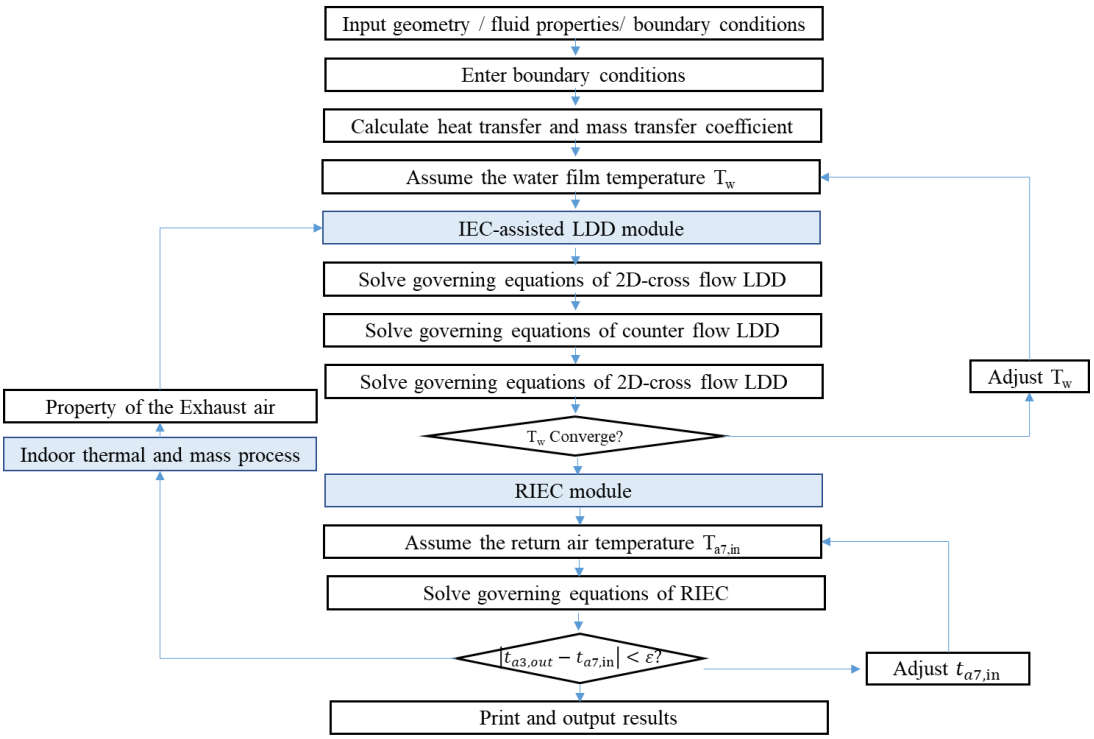

Figure 3 Simulation flow chart for solving the ICLDAC model

2.2.1. *LDD* model

The dehumidification channel and the internal cooling channel in the internal cooling *LDD* model were built as a 2-dimensional finite model. To improve the heat exchange between the dehumidification and cooling channels, a hexagonal heat exchanger was used. The latent and sensible heat processes of the microelements in the dehumidification channel can be described as Eq. 1-2.

$$dQ_{sen,s} = \alpha_s(t_s - t_{a1})2A\frac{d_x}{l} \tag{1}$$

$$dQ_{lat,s} = \frac{\alpha_s}{c_{p,a1}} \cdot r_w \cdot (w_s - w_{a1})2A\frac{d_x}{l} \tag{2}$$

The energy and mass conservation equations for dehumidification channels (Eq.3-4.) and for the internal cooling channel (Eq.5-6) in the *LDD* can be expressed, respectively.

$$Qdx + m_{a1}dh_{a1} - dm_s c_{ps} t_s = 0 \tag{3}$$

$$m_{a1}dw_{a1} = dm_s \tag{4}$$

$$-Qdy + m_{a5}dh_{a5} - dm_w c_{pw} t_w = 0 \tag{5}$$

$$m_{a5}dw_{a5} = dm_w \tag{6}$$

The heat transfer between the two channels can be expressed as Eq. 7.

$$Q = K(t_s - t_w)d_x d_y \quad (7)$$

2.2.2. $RIEC$ model

A 2-dimensional finite model was created for the $RIEC$. As the air receives adequate latent heat treatment before entering the $RIEC$, it is presumed that there is only sensible heat exchange taking place in the $RIEC$ rather than condensation. The heat and mass balances and the mechanisms of heat and mass transfer (Eq. 8-10) of the primary and secondary channels of the model will be solved.

$$\alpha_{a7}(t_{wall} - t_{a7})dA = c_{pa7}m_{a7}dt_{a7} \quad (8)$$

$$\alpha_{ma7}(\omega_{twall} - \omega_{a7})dA = m_{a7}dw_{a7} \quad (9)$$

$$\alpha_{a2}(t_{a2} - t_{wall})dA = cp_{a2}m_{a2}dt_{a2} \quad (10)$$

The mass balance of the evaporation film in the secondary channel and the energy balance equation of the control volume are shown in Eq. 11-12.

$$dm_{ew} = m_{a2}dw_{a2} \quad (11)$$

$$m_{a2}dh_{a2} - cp_{a2}m_{a2}dt_{a2} = d(cp_{wall}t_{ew}m_{ew}) \quad (12)$$

The air pressure in the room remains constant, and the fresh air from RIEC sent into the room is consistent with that exhausted to *LDD*. The mass flow rate relationship between the secondary channels of the *RIEC* and *LDD* depends on the extraction air ratio of the *RIEC* re,$re = \frac{m_7}{m_3}$. The airflow ratio between the internal cooling channel and the dehumidification channel in the LDD expressed as RCD, $RCD = \frac{m_5}{m_1}$.

2.2.3. System model validation

The accuracy of the developed numerical models of the main components of the $LDAC$ has been verified by two published research works respectively. They are experiments on a $RIEC$ [27] and simulations on an LDD with built-in indirect evaporative cooling as internal cooling [28].

The simulation results of LDD were compared with a study using *IEC* as the internal cooling for LDD. The numerical model developed by Saman and Alizadeh [28] investigated the outlet

temperature and humidity of primary air obtained by internally cooled LDD treatment under different mass flow rates. By setting the same primary and secondary inlet air conditions (33°C, 0.171 kg/kg; 27°C, 0.100 kg/kg) and operating conditions (m_{a1}=0.42 kg/s, v_{a1}=1 m/s, RCD=1) as reported in the literature. The dehumidification and cooling performance of the two models at different solution mass flow rate is shown in Figure 4. A difference of 1.5-6.3% was found between the results of the newly developed model and the literature.

Experiments by Riangvilaikul and Kumar [27] applying part of treated primary air directly as a source of secondary air in IEC were used to validate the cooling performance of the $RIEC$ model. The extraction ratio (re) was introduced as an indicator of the ratio of primary to secondary air. To verify the accuracy of the current numerical model, the inlet air conditions (re=0.33, v_{a1}=2.4 m/s, t_w=28 °C) and geometric parameters (h=0.005m, A_w=0.08 m, A_h=1.2m) of the previous model were applied to the current model and simulated in same flow pattern. Comparing the $t_{a1,out}$ of the current model with the model of Riangvilaikul and Kumar (Figure 5), the statistics show a difference in the outlet temperature between 0.9% and 10.0%.

Numerical model comparison results show an error between the predicted values and experimental data in the range of 2.4 % to 16.3%, based on an acceptable discrepancy between the developed model and published results. Current models can predict outlet temperature and humidity for LDD and $RIEC$ models.

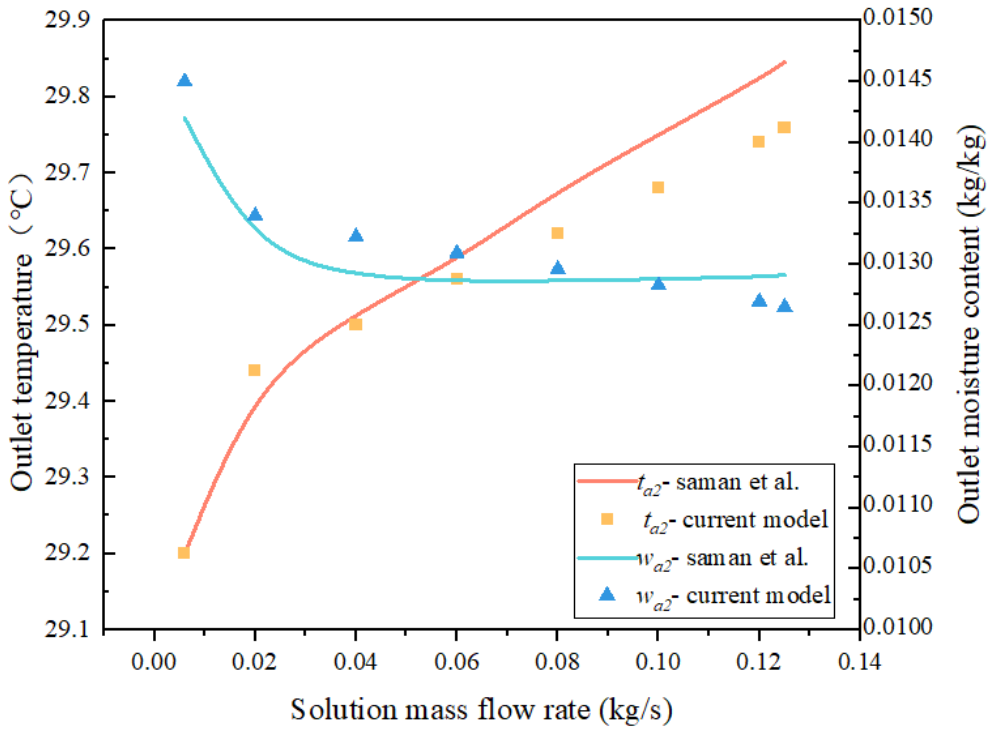

Figure 4 Comparison of LDD simulation results with published simulation model [28] for model validation

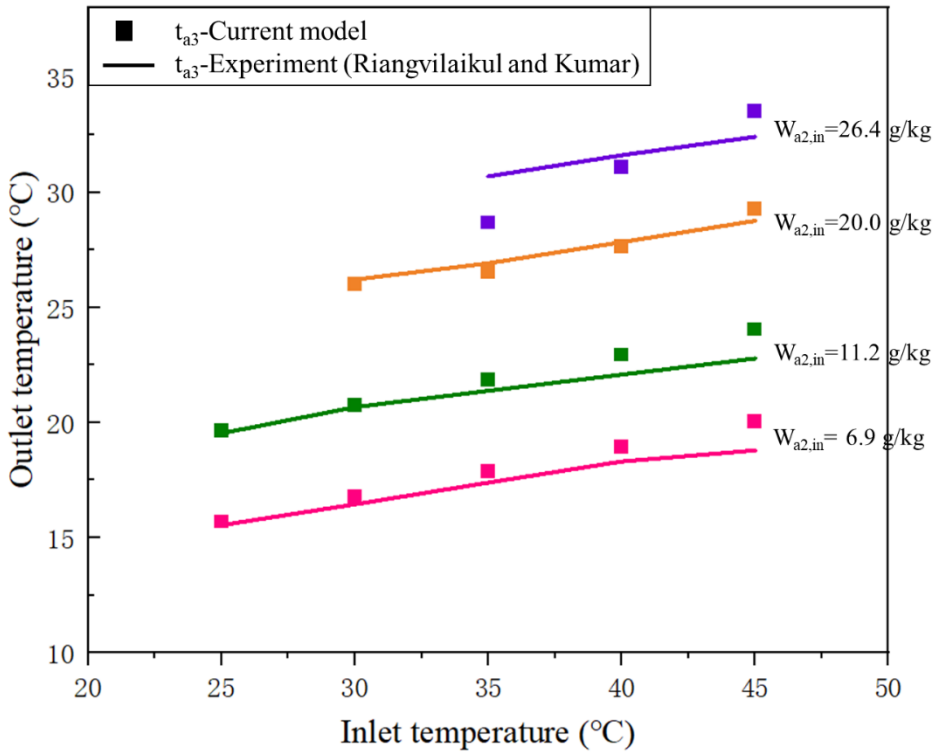

Figure 5 Comparison of RIEC simulation results with published simulation model [27] for model validation

3. Methodology

3.1.Development of optimization strategy with RSM

The objective of design optimization in this study was to determine the optimum combination of key design parameters that will maximize the cooling and dehumidification performance of the system. The overall workflow of the system performance and optimization strategy for the $ICLDAC$ system is shown in Figure 6. The process included system modeling, regression analysis, response surface method (RSM), performance evaluation, and optimization. The mathematical model of the $ICLDAC$ system was first developed and experimentally validated. The simulations developed in Section 2 provided data to develop the response surface models. Based on a multi-factor analysis of variance ($ANOVA$), the variables that significantly affect the performance of the $ICLDAC$ system were identified. The response surface method was used to model six parameters corresponding to three responses: cooling capacity (Q), latent heat removal rate (Q_{lat}), and dehumidification efficiency (η_d) as response values. Models based on the RSM were used to predict the performance of the $LDAC$ system over the entire range of constraints and discover the relationship between system parameters and performance. The monthly optimized operational scheme based on the environmental parameters in Hong Kong was established using the desirability function approach (DFA).

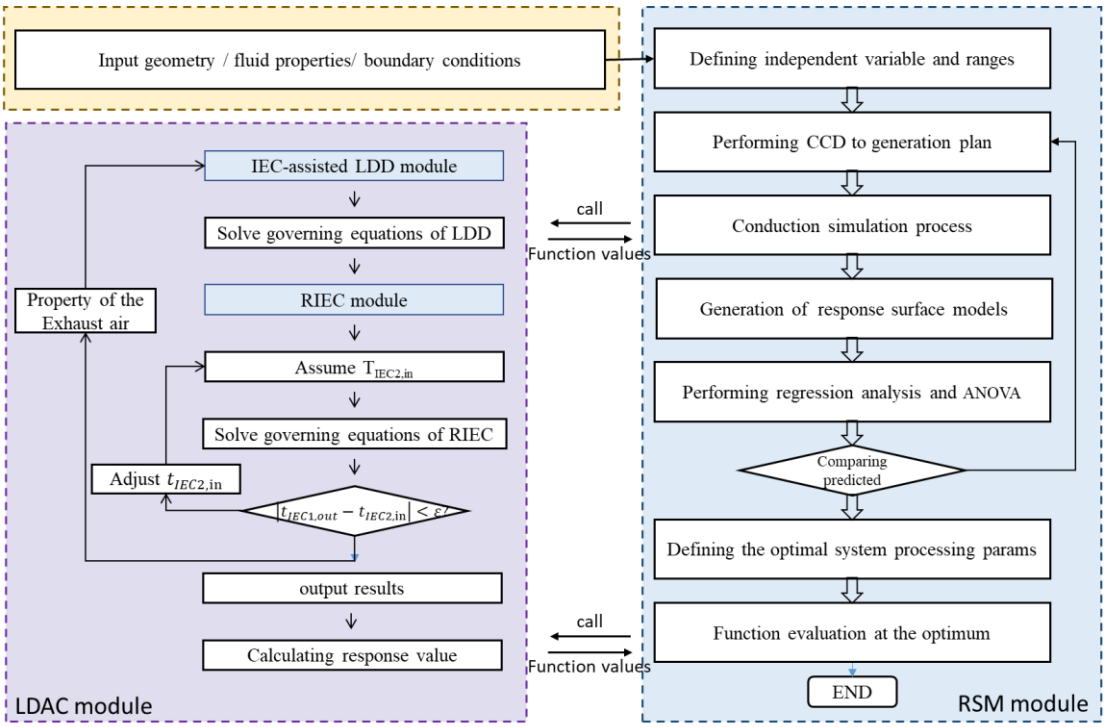

Figure 6 Flowchart of the proposed methodology to optimize the ICLDAC system

Once the range of the critical factors has been identified, it is necessary to ascertain the values of the elements and consider their interactions. *RSM* enables the development of a mathematical model that includes primary, quadratic, and interaction terms between any two factors through a reasonably limited number of tests. The *RSM* process in this study included the selection of the influencing and independent variables, execution of the designed simulation experiments, determining a response surface model based on the simulation results, and assessing the validity of the obtained model.

The central composite design (CCD) was employed to formulate the simulation scheme. Table 2 shows the experimental arrangement for the 3-level evaluation of six independent variables (k = 6), including environmental parameters: temperature (t_{a1}), relative humidity (RH_{a1}), operational parameters: inlet air velocity (v_{a1}), the concentration of the desiccant (x_s), secondary to the primary air flow ratio in LDD (RCD), and design parameter: number of transfer units of the plate heat exchanger (NTU). These models can accurately explore the relationship between each factor and the response value and efficiently determine the optimal

condition of the multi-factor system. The selection of the main influencing variables was based on the parameters that appeared significant in the results of the multivariate variance to develop the response surface model. As a dimensionless parameter for heat transfer capacity, it is important to note that the NTU values were varied in terms of channel length and flow rate to ensure the independence of the parameters. The threshold of the parameters selected for testing was based on the results of previous studies and environmental parameters in hot and humid regions [8, 29]. The concentration of desiccant was chosen concerning the dissolution capacity of the desiccant. This study used the second-order polynomial model given in the equations (Eq. 13) as the response surface model. The multi-objective optimization of the response surface model was then used to determine the optimal design. The optimization approach used simultaneous optimization [30] with the desirability function approach (DFA) by Derringer and Suich [31]. FDA is achieved by first transforming each response (y_i) combined with the willingness weight (r) into a single function (d_i) that varies over its range of values ($F-T$) (Eq. 14). The design variables are then chosen to maximize the overall desirability (D) (Eq.15). Using *DFA* to optimize the system fitted by the regression equation, the optimal operating parameters for different input environmental conditions can be determined.

$$y = \alpha_0 + \sum_{i=1}^{j}\alpha_i x_i + \sum_{i=1}^{k}\alpha_{ii} x_i^2 + \sum_{i=1}^{i<j}\alpha_{ij} x_i x_j \tag{13}$$

$$d = \left(\frac{y-l}{T-l}\right)^r, L \geq y \geq T \tag{14}$$

$$D = (d_1 d_2 \cdots d_n)^{\frac{1}{n}} \tag{15}$$

Table 2 The parameter ranges designed for the response surface method

Name (Units)	t_{a1} ℃	RH_{a1} kg/kg	v_{a1} m/s	x_s %	*RCD* %	*NTU* -
Minimum	24	60	1	0.25	0.5	1
Maximum	40	80	3	0.45	0.9	5

3.2. Performance indicators

The indicators to evaluate the performance of the *ICLDAC* include cooling capacity (C), latent heat removal rate (Q_d) and dehumidification efficiency (η_d). They are calculated as Eqs.16-18,

respectively. η_d is used as an evaluation index that assesses the dehumidifying efficiency of a dehumidifier. It is defined as the ratio of the primary air humidity variation value to the dehumidification potential of the fresh air and desiccant solution in the saturated state.

$$C = m_{a4} \cdot (h_{a4} - h_{a1}) \tag{16}$$

$$Q_{lat} = r_w \cdot m_{a4}(w_4 - w_1) \tag{17}$$

$$\eta_d = (w_1 - w_4)/(w_1 - w_{es}) \tag{18}$$

4. Results

4.1. Regression analysis and *ANOVA* for response values

An analysis of variance ($ANOVA$) of the responses obtained from the $ICLDAC$ system simulations allowed for identifying important parameter terms. The validated numerical model tested 86 groups of case trials according to a central composite design (CCD) and responses (C, Q_{lat}, η_d) was calculated.

The responses represented by $\eta_d, C, and\ Q_{lat}$ reveal the cooling and dehumidification capability and efficiency of the system. The results (App. A) show that all six parameters significantly impact the responses of $C\ and\ Q_{lat}$. When the six factors interact in pairs, the impact of the intersection term on the responses varies in magnitude. Most of the intersection terms have a significant effect on the cooling capacity of the system. However, the interaction between x_s and NTU value was not prominent. The Q_{lat} is significantly affected by the pairwise interaction between the inlet air condition and the x_s, RC, and NTU, respectively. There are not many intersection parameters affecting dehumidification efficiency: except for inlet air conditions, the correlation between NTU and v_{a1} has a very significant impact on dehumidification efficiency (p-value<0.001).

4.2. Predicted models of output responses

In this section, a response surface model for predicting the objective function was developed based on the simulation results for different environmental and operating parameters. Based on the CCD, 86 models were calculated using validated numerical models. Multiple regression analysis was performed on the three responses and the corresponding six factors. The Bayesian

information criterion [30] was used for model fitting. The backward selection was employed for training feature values. This study used a second-order polynomial model as the response surface model. Equation 19-21 gives the quadratic response surface equation that combines the regression coefficients in encoded form to represent the objective function.

$$\begin{aligned} C = {} & 5.97 + 1.71 * t_{a1} + 0.3299 * RH_{a1} + 0.9183 * v_{a1} + 0.4031 * x_s + 1.09 * RCD \\ & + 0.8584 * NTU + 0.0754 * t_{a1}RH_{a1} + 0.2298 * t_{a1}v_{a1} + 0.3474 \\ & * t_{a1}RCD + 0.2599 * t_{a1}NTU + 0.0846 * RH_{a1}NTU + 0.824 * RH_{a1}RC \\ & + 0.0283 * v_{a1}x_s + 0.1749 * v_{a1}RCD + 0.172 * v_{a1}NTU + 0.0994 \\ & * x_sRCD + 0.1.1 * x_sNTU + 0.1567 * RCDNTU + 0.1163 * t_{a1}^2 \\ & - 0.0764 * v_{a1}^2 - 0.0454 * x_s^2 - 0.1029 * NTU^2 \end{aligned} \tag{19}$$

$$\begin{aligned} Q_{lat} = {} & 3.44 + 1.05 * t_{a1} + 0.3341 * RH_{a1} + 0.2691 * v_{a1} + 0.4064 * x_s + 0.8121 \\ & * RCD + 0.8323 * NTU + 0.0766 * t_{a1}RH_{a1} + 0.0829 * t_{a1}v_{a1} \\ & + 0.2490 * t_{a1}RCD + 0.2501 * t_{a1}NTU + 0.0236 * RH_{a1}v_{a1} + 0.0823 \\ & * RH_{a1}RCD + 0.0834 * RH_{a1}NTU + 0.0311 * v_{a1}x_s + 0.1017 * v_{a1}RCD \\ & + 0.1524 * v_{a1}NTU + 0.0995 * x_sRCD + 0.0998 * x_sNTU + 0.1533 \\ & * RCDNTU + 0.1173 * t_{a1}^2 - 0.064 * v_{a1}^2 - 0.0461 * x_s^2 - 0.0.0986 \\ & * NTU^2 \end{aligned} \tag{20}$$

$$\begin{aligned} \eta_d = {} & 0.4905 + 0.0003 * RH_{a1} - 0.0860 * v_{a1} - 0.0012 * x_s + 0.0474 * RCD \\ & + 0.1161NTU - 0.0032 * v_{a1}RCD - 0.0090 * v_{a1}NTU + 0.0047 \\ & * RCDNTU + 0.0150 * v_{a1}^2 - 0.0029 * RC^2 - 0.0139 * NTU^2 \end{aligned} \tag{21}$$

Multiple regression analysis was performed on six parameters and three response values. The p-value indicates the probability of obtaining a test statistic at least as extreme as the observed statistic. The F-test assessed significance statistics for the three obtained response surface models at 95% confidence. Regression models with high F-values and p-values less than 0.05 were considered sufficient to predict the response.

Table 3 reveals the accuracy of the response surface models. The results show that the

coefficients of determination (R^2) for C, Q_{lat}, $and\ \eta_d$ are 0.9969, 0.9980, and 0.9990, respectively. The data predicted by the model matches well with the test data, indicating that the response of each factor can be predicted based on the simplified quadratic model and factors value entered into the model, which can be used to optimize the design and operation of the $LDAC$ system.

Table 3 Regression analysis for responses

Response	Order	P value	R^2	Adjusted R^2
Q_{lat}	Quadratic	<0.0001	0.9980	0.9929
C	Quadratic	<0.0001	0.9969	0.9956
η_d	Quadratic	<0.0001	0.9990	0.9976

4.3. Two-factor analysis and parameter optimization

The developed predictive model can predict the response values by various factors and be used to optimize the $ICLDAC$ parameters. The six parameters involved in this system contain the environmental factors ($t_{a1}\ and\ RH_{a1}$), design factor (NTU), and the operational parameters (v_{a1}, x_s, RCD). Operating parameters can be flexibly changed during system optimization to adjust the system performance. Complex systems have more than one operating parameter. Single-value regulation has limited ability to improve system performance. An integrated exploration of the crossover effects between factors and responses may maximize the benefits of system optimization. This section used a two-factor interaction analysis to optimize the operational parameters. The results can be used to guide the operational settings of the proposed $LDAC$ system. The optimized values of the operating parameters can be further applied to different environmental parameters of the Hong Kong air-conditioning month for the case study.

4.3.1. Effects of inlet air velocity and solution concentration on system performance

Figure 7 shows the effect of solution concentration (x_s) and inlet air flow rate (v_{a1}) on the latent heat removal rate (Q_{lat}) and cooling capacity (C) for a fixed RCD. High wind speed and high-concentration solution positively affect the latent heat removal rate of the system. However, raising the wind speed to 2.5 m/s based on a medium wind speed (2.0 m/s) does not considerably enhance Q_{lat} when the system is operating in a high-concentration solution (x_s=0.4). This

phenomenon is attributed to the fact that the greater x_s, the lower the partial pressure of the water vapor at the solution film. That leads to a larger mass transfer drive. Nevertheless, when the system operates at high v_{a1}, the high concentration of dehumidifier fails to fulfill its dehumidifying potential. The simulation results for the response of cooling capacity at various v_{a1} and x_s are shown in Figure 6-b. The cooling capacity consists of sensible and latent heat changes. Changing the v_{a1} has a more significant effect on the response compared with the result by adjusting the x_s. This phenomenon would be attributed to more air volume being handled. When the system is operated with the same x_s (0.4) and a raising v_{a1} from 1.5 to 2.5m/s, the total cooling capacity can reach 7.20 kW.

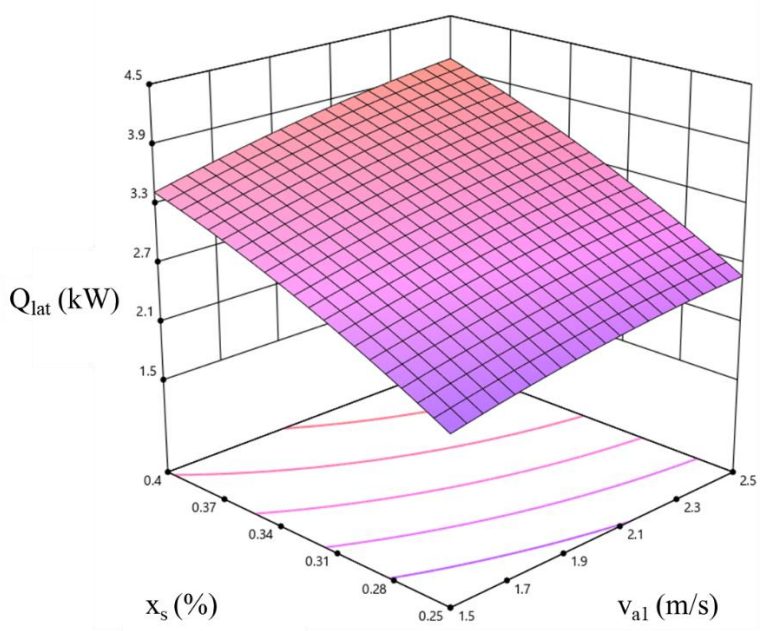

(a)

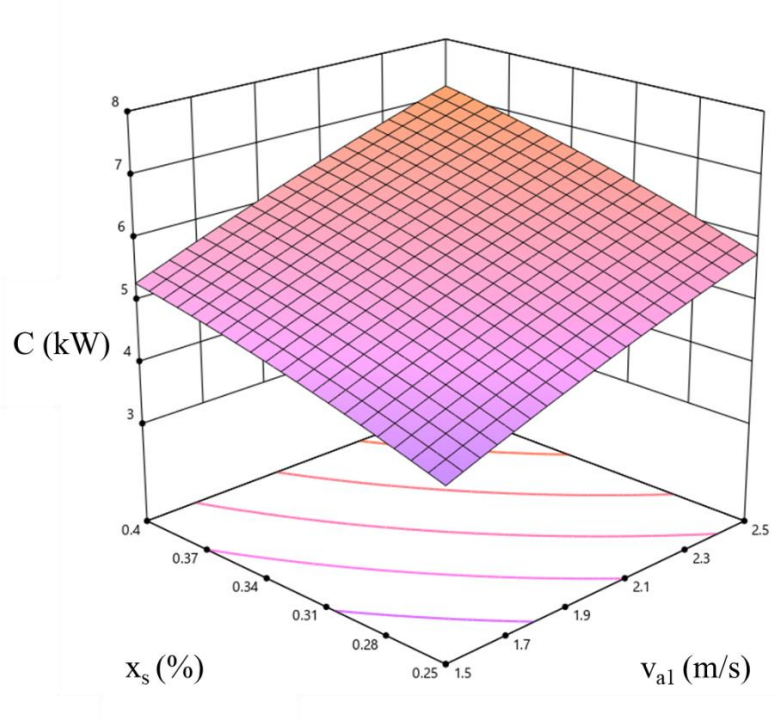

(b)

Figure 7 Response surface for latent heat removal rate (a) and cooling capacity (b) versus desiccant concentration and inlet air velocity at NTU= 3, $RHa1$ =70%, RCD= 0.7, and $Ta1$= 32 °C.

4.3.2. Effects of inlet air velocity and LDD secondary to primary air ratio on system performance

The findings in the preceding section demonstrate that, at a given RCD of the system, increasing v_{a1} has limited ability to improve Q_{lat}. This result is due to the short contact time between the air and the dehumidifying solution. The water vapor is not removed sufficiently, resulting in low dehumidification efficiency. Figure 8 shows the response of cooling capacity (C) and dehumidification efficiency (η_d) under the influence of v_{a1} and RCD. In contrast to the result of dehumidification efficiency, the C (Figure 8-a) of the system performs better at high air velocity. For the system operating at high RCD (RCD=0.8), the change in v_{a1} had a more significant effect on the responses: C increased by 2.19 kW. This phenomenon is due to more amount of air being processed. Another reason might be that the larger amount of inlet air enhances the evaporative cooling capacity in the secondary channels. Consequently, increasing the room exhaust air rate can positively affect C. The system showed a better η_d

at low v_{a1} and high RCD. These results corroborate the ideas of Riangvilaikul and Kumar [27], who suggested that a larger extraction ratio (re) in $RIEC$ helps to increase the cooling efficiency. However, consideration should also be given to the reduction in the flow rate of useful air supplied to the cooling space. Sacrificing more produced air to feed back into the $RIEC$ would cause insufficient fresh air to handle indoor loads and weaken the internal cooling effect of internal cooling in the LDD.

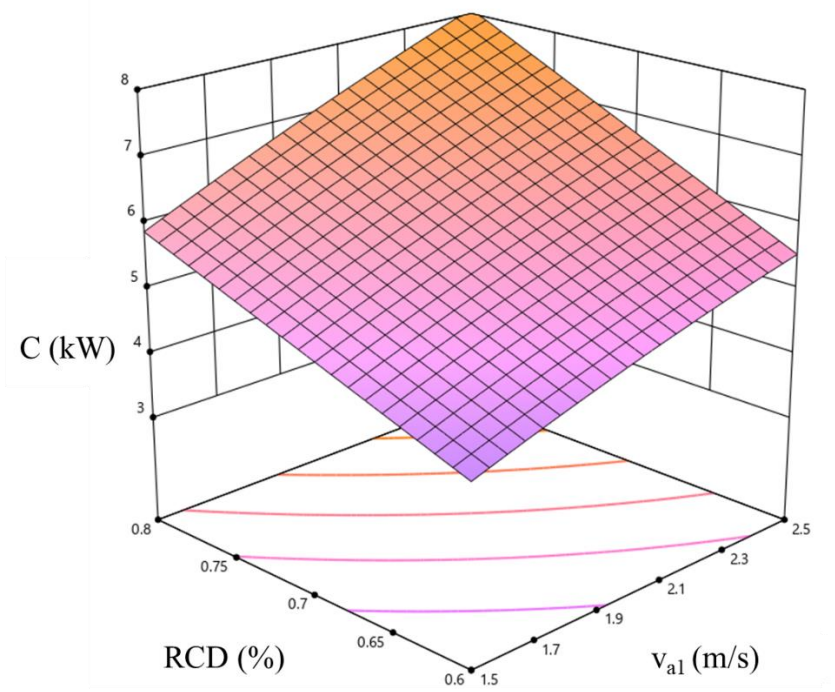

(a)

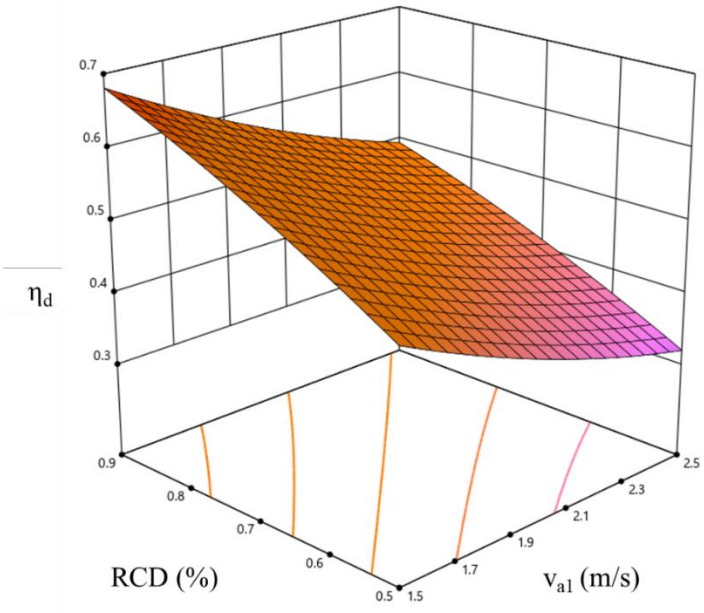

(b)

Figure 8 Response surface for cooling capacity (a) and dehumidification efficiency (b)

versus RCD and inlet air velocity at NTU= 3, RH_{al} =70%, x_s= 0.35, and T_{al} = 32 °C.

4.3.3. Effects of solution concentration and LDD air flow ratio on system performance

Figure 9 illustrates the effect of solution concentration (x_s) and secondary to primary air flow ratio in LDD (RCD) on the cooling capacity (C) and latent heat removal rate (Q_{lat}) of the system when the inlet air velocity is a fixed value (2.0m/s). It is noticeable that a higher x_s achieves better cooling and dehumidification capacity. The RCD also shows a positive correlation to the response value of C and Q_{lat}. The higher RCD in the LDD, the better the internal cooling effect can be achieved. When operating with a high x_s, increasing the RCD to enhance the internal cooling of the LDD has a particularly significant impact on improving the Q_{lat} of the system. In the newly developed response surface model, when RCD is increased from 0.6 to 0.8 with x_s kept at 0.4, the corresponding Q_{lat} increases from 2.92 kW to 4.74 kW: a rise of 62.3%. This phenomenon may be explained by the increased proportion of working air in the LDD, which helps the LDD achieve better internal cooling to ensure better dehumidification efficiency. Figure 9-b shows the overall effect of the two-factor model (RCD, x_s) on the response of the latent heat removal rate. Regarding the response surface model of the cooling capacity, C is positively correlated with the two factors. However, increasing the RCD ensures better dehumidification performance of the LDD, but a proportion of the airflow for indirect evaporative cooling of the $RIEC$ is sacrificed. A significant increase in cooling capacity from 5.14 to 7.51 can be observed by increasing the RCD from 0.6 to 0.8 when the system is operated at high x_s (0.4). The trade-off between dehumidification and cooling capacity makes RCD less effective in improving response at a low x_s than in high x_s systems. In the practical application of the model, therefore, in addition to optimizing the operating parameters, the demand for dehumidification and cooling capacity under different atmospheric conditions should also be considered.

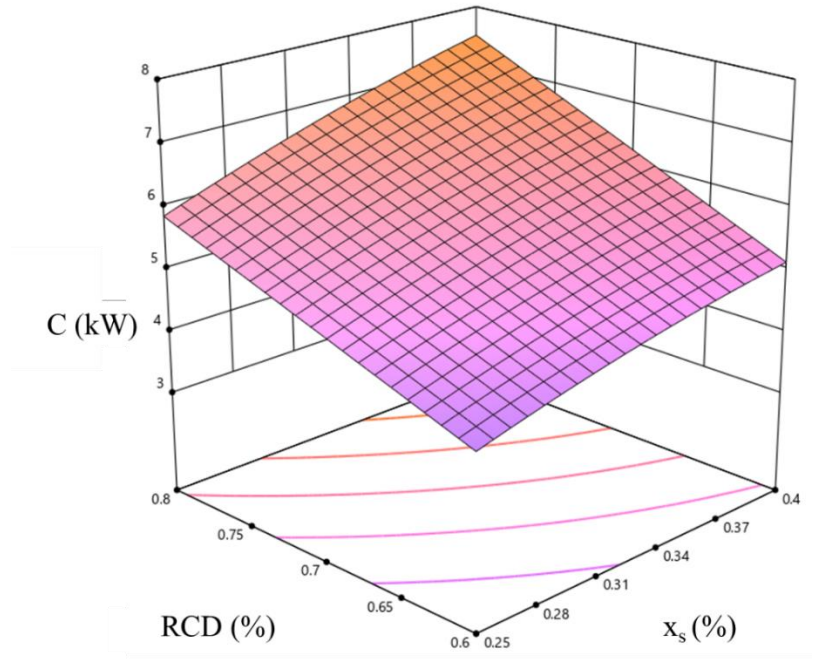

(a)

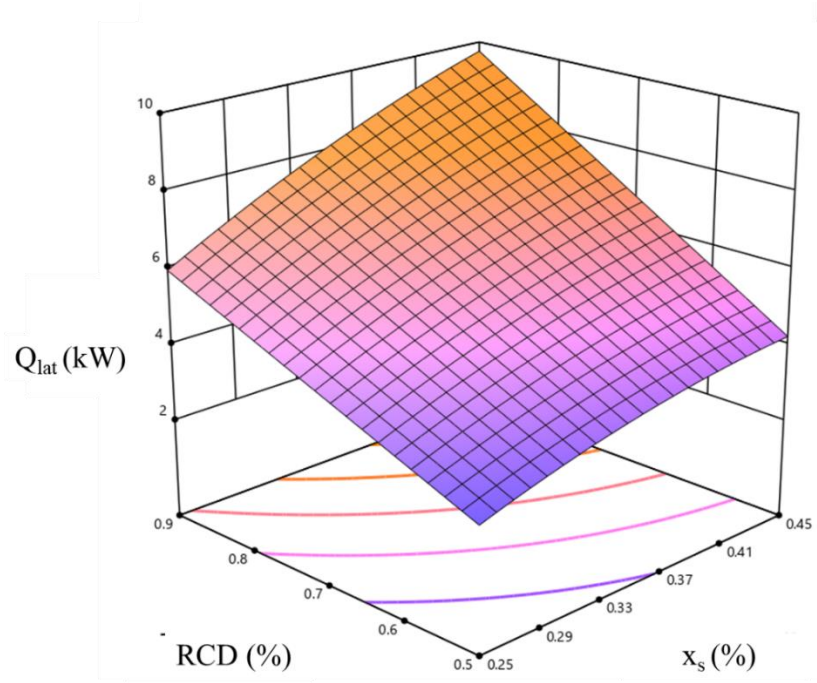

(b)

Figure 9 Response surface for cooling capacity(a) and latent heat removal rate (b) versus desiccant concentration and LDD air flow ratio at *NTU*= 3, RH_{a1} =70%, v_{a1}=2.0, and t_{a1}= 32 °C.

4.4. Application optimization schemes in typical operating environments

Among the parameters that affect system performance, operating parameters are often related

to the outdoor air conditions in which the system is located. This section applies the prediction model (Eq.18-20) generated by RSM, considering the optimized operating parameter values under different inlet air conditions. According to the meteorological data, the newly developed response surface model was used to calculate the optimal operational parameters under different air inlet parameters and evaluate the system performance. The multi-objective optimization problem with three responses (Q_{lat}, C, η_d) was explored by DFA. The responses were transformed into a non-dimensional quantity. By setting the weight equal to 1, the linear desirability function (d) was established. In this section, the cooling and dehumidifying performance of both monthly optimized parameters and the previously recommended operation scheme based on the typical outdoor weather of Hong Kong were all explored to tackle the system optimization.

The meteorological data given in Table 4 is derived from the Tung Chung Meteorological Station in Hong Kong. The inlet air temperature and relative humidity are obtained from the average of the monthly office hours (7 am-7 pm) of the observatory during the 17 years from 1998 to 2015. Many previous design schemes were based on the typical summer design conditions in Hong Kong (33 ℃, 73%) [32]. To meet the air intake conditions of high temperature and humidity, the previous system research in Hong Kong [33] recommended the operation plan to set a high concentration of the desiccant solution (x_s=0.4%) for the whole year and cooperate with low air speed (v_{a1}=1.5m/s) and 0.7 of RCD to ensure better dehumidification efficiency. However, the temperature and humidity conditions in Hong Kong vary significantly from April to October. Monthly optimization might improve the effectiveness of the system operation throughout the year. Table 4 also shows the predicted month-by-month optimization parameters based on the response surface model and desirability function. This plan makes the system have ideal dehumidification and cooling effect every month and achieves lower supply air temperature and moisture content. Although the higher the NTU, the better the performance of the system. But NTU is limited by the material of the PHE. The model parameters were set according to a heat exchanger (NTU=4.0, h=0.004m, A_w=0.4m). It is assumed that the secondary air of the LDD comes from the exhaust air (T_{a5}=25°C, RH_{a5}=55%). Combining the response surface model with monthly meteorological data can give

the recommended optimal operational parameters for different months.

Table 4 Monthly optimized operational parameters (compared with the previous scheme: v_{a1}=1.5 m/s, x_s=0.4, RCD=0.7)

Environmental Parameters			Optimized Operating Parameters		
Month	t (℃)	RH (%)	v (m/s)	x_s	RCD
4	24.7	75.3	1.5	0.4	0.8
5	27.9	78.8	1.5	0.4	0.8
6	29.7	75.5	2	0.4	0.75
7	30.7	73.2	2	0.4	0.75
8	30.5	74.8	2	0.4	0.7
9	31.4	73.4	2	0.4	0.7
10	27.5	64.1	1.5	0.4	0.7

The monthly weather conditions and the corresponding optimized system sensible heat rate (SHR) are shown in Fig. 10. Before optimization, the variation of SHR in single operation mode of $ICLDAC$ is slight, within 10%. The monthly optimized SHR is 36.4.0%-41.0% in the hot and humid months and 20.5% and 27.3% in April-May. This improvement is achieved by changing the RCD to distribute the re in the $RIEC$ and varying the va1. Monthly optimization applies operational schemes with different SHRs in areas with large heat and humidity changes. The new system and optimization strategy will reduce energy consumption in high-humidity areas compared to traditional AC air conditioners that simultaneously handle heat and humidity loads. Compared with the $LDAC$ device that directly mixes the return air, which will cause insufficient fresh air when it uses a smaller SHR [11], the newly proposed system breaks the limitation of high SHR operation in areas with high fresh air and high dehumidification requirements.

The optimization results give a recommended operating inlet air velocity between 1.5m/s and 2.0m/s in summer and a recommended RCD of 0.7-0.8 in summer. The comparison of the cooling and dehumidification performance between the $ICLDAC$ monthly optimization scheme and the previous design and operation scheme [9, 33] is shown in Figure 11. The η_d in April and May has significantly improved 7.5% and 7.3%, respectively. When the removed moisture is guaranteed, better dehumidification efficiency can reduce waste and ensure efficient

system operation. Among the contributions of each factor to the response of η_d, $the\ v_{a1}$, and the cross-term of $v_{a1} * RCD$ play a critical role in the value of η_d. The η_d is improved by setting high RCD (0.8) and low v_{a1} (1.5m/s). This optimization result is consistent with the two-factor analysis in section 4.3.2: High-concentration desiccant can achieve dehumidification during high-humidity months. However, η_d will be slightly impaired because of the high dehumidification potential. High RCD (0.8) allows the system to maintain high η_d even at higher x_s.

The system operated with optimized parameters has improved C and Q_d significantly from April to October (Figure 10). Total cooling capacity peaks in July ($C = 7.448\ kW$) with a 23.61% improvement over the model without optimization by DFA. According to Section 4.2, in addition to temperature, the v_{a1} has the largest contribution to the C and Q_d among all first-order operational items, and they are all positively correlated. By increasing the v_{a1} $(2.0\ m/s)$ in high-temperature months, although the η_d has been reduced due to the shortened contact time between desiccant and primary air, and the dehumidification capacity of the system has not been impaired. However, the system achieves better C and Q_{lat}, and more fresh air is sent indoors to handle the indoor heat and moisture loads. The optimized model achieved a 20.7% increase in latent heat removal rate in April. For the empirical equation fitted in Section 4.2, RCD is one of the operating parameters that play a decisive role for Q_{lat}. RCD is positively related to Q_d, which determines the distribution relationship between the airflow for sensible cooling at RIEC and the internal cooling for LDD after handling the indoor heat and humidity load. Increasing the RCD would be a promising option in warm and humid months when there is a demand for latent heat removal rate from the system.

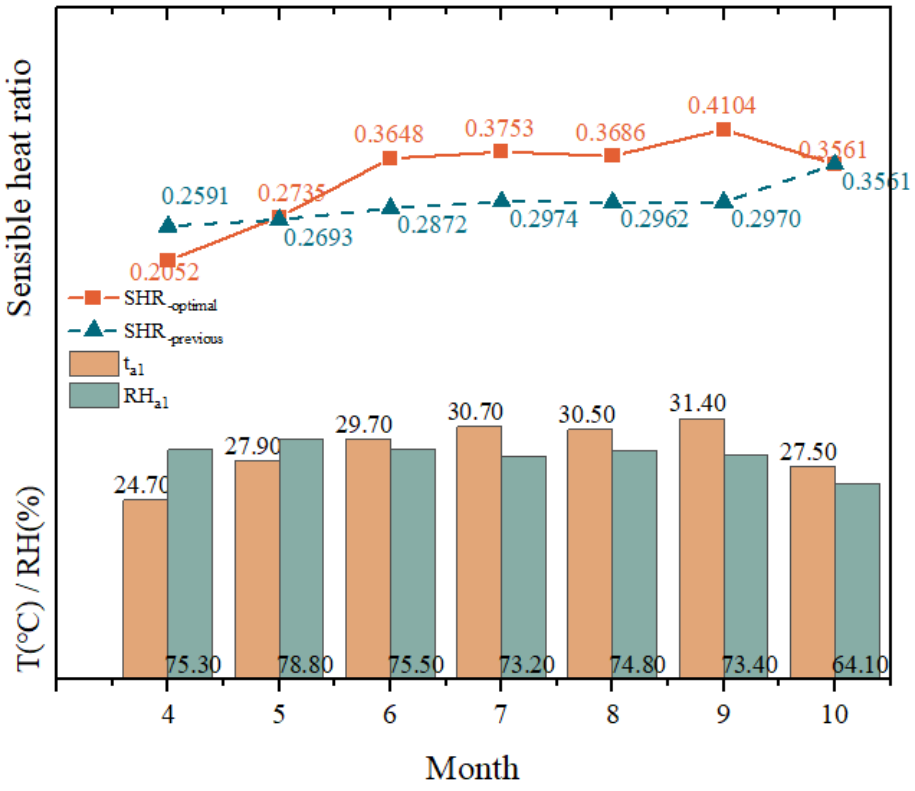

Figure 9 Monthly average meteorological parameters and sensible heat ratios for two operating schedules in Hong Kong

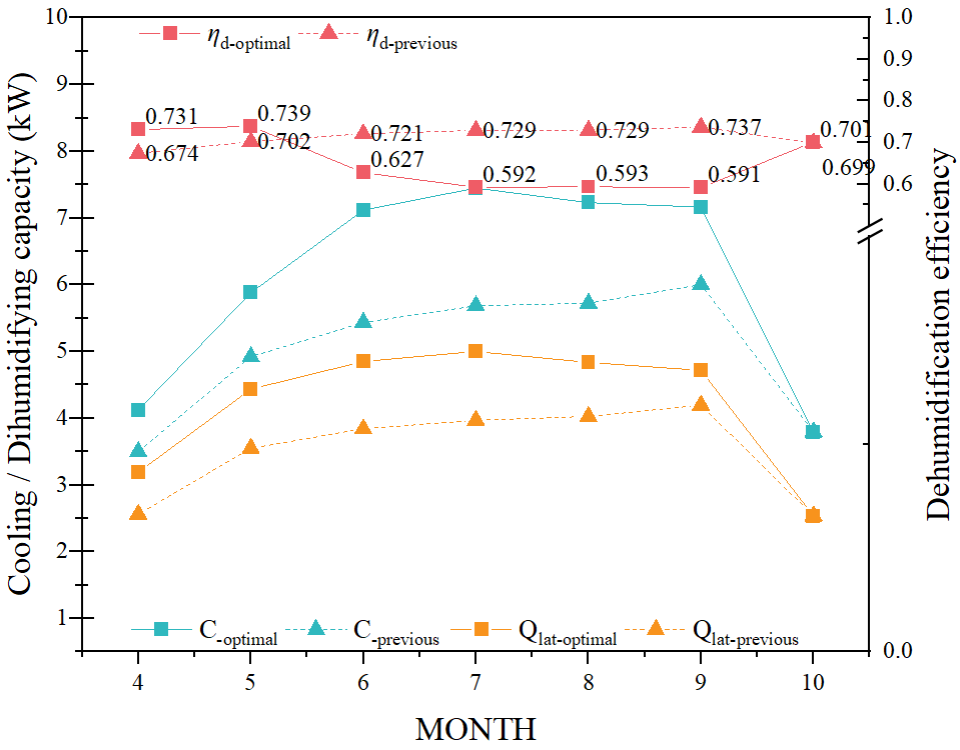

Figure 11 Monthly optimization results of the $ICLDAC$ system in Hong Kong from April to October applying the newly proposed operation strategy based on RSM: Dehumidification

efficiency, cooling capacity, and latent heat removal rate

5. Conclusions

This study investigated an effective multi-objective optimization method for an internally cooled liquid desiccant air conditioning system ($ICLDAC$) to identify system configurations for maximizing the system performance. The system is designed to provide sufficient fresh air intake and capture the waste heat energy of the exhaust air indirectly without impairing the energy performance of the system. The main components (LDD and $RIEC$) can basically realize the decoupling of the heat and humidity loads and independently handle the cooling and dehumidification needs of different months. The main results are highlighted below.

(1) The response surface models for the $ICLDAC$ performance prediction were developed using the numerical models and response surface method (RSM). The simulation results from the validated mathematical model were regressed, and a response surface model was generated. The desirability function was used to tackle the system multi-objectives optimization problem. The wind speed has the most significant impact on enhancing the performance of the system. The results of the two-factor analysis of the operating parameters showed that the system operating at a low wind speed (v_{a1}=1.5m/s) and high RCD (0.8) could maintain a higher dehumidification efficiency (η_d=0.75) when the solution concentration was higher (x_s=0.40).

(2) The 17-year monthly meteorological data of Hong Kong was used in the empirical model to explore the regional applicability of the $ICLDAC$. The results of multi-objective optimization suggest that in April and May, the operation plan of high exhaust air and low wind speed should be adopted, and the latent heat removal rate of the optimized system can be increased by 20.8%. By raising air velocity to 2.0 m/s and cutting down the secondary to primary air ratio and solution concentration to 80% and 0.4 in the warmer months, the peak cooling capacity is 7.448 kW, which increased by 23.6%.

(3) The RSM and DFA enable performance predictions and optimization for $ICLDAC$ system. This optimization scheme might precisely regulate cooling and dehumidification by decoupling the heat and humid load and conducting the targeted design. It is expected to expand

the application and climate adaptation analysis of internally cooled LDD and $RIEC$ to a broader region.

Acknowledgment

The work described in this paper was supported by grants from the Research Grants Council of Hong Kong (with grant numbers UGC/FDS24/E03/20 and UGC/IDS (24)/20).

References

1. Allison, C.K. and N.A. Stanton, *Eco-driving: the role of feedback in reducing emissions from everyday driving behaviours.* Theoretical Issues in Ergonomics Science, 2019. **20**(2): p. 85-104.
2. Pérez-Lombard, L., J. Ortiz, and C. Pout, *A review on buildings energy consumption information.* Energy and Buildings, 2008. **40**(3): p. 394-398.
3. Department, C.a.S., *Hong Kong Energy Statistics Annual Report*. 2021, Census and Statistics Department.
4. Bakker, A., et al., *Building and environmental factors that influence bacterial and fungal loading on air conditioning cooling coils.* Indoor air, 2018. **28**(5): p. 689-696.
5. Gu, Y., et al., *Aqueous lithium chloride solution as a non-toxic bactericidal and fungicidal disinfectant for air-conditioning systems: Efficacy and mechanism.* Environmental Research, 2022. **212**: p. 113112.
6. Luo, Y., et al., *Experimental and theoretical research of a fin-tube type internally-cooled liquid desiccant dehumidifier.* Applied Energy, 2014. **133**: p. 127-134.
7. Zhang, Y., et al., *Counter-crossflow indirect evaporative cooling-assisted liquid desiccant dehumidifier: Model development and parameter analysis.* Applied Thermal Engineering, 2022. **217**: p. 119231.
8. Chen, Y., Y. Luo, and H. Yang, *Energy Saving Potential of Hybrid Liquid Desiccant and Evaporative Cooling Air-conditioning System in Hong Kong.* Energy Procedia, 2017. **105**: p. 2125-2130.
9. Chen, Y., H. Yang, and Y. Luo, *Investigation on solar assisted liquid desiccant dehumidifier and evaporative cooling system for fresh air treatment.* Energy, 2018. **143**: p. 114-127.
10. Kim, M.-H., J.-S. Park, and J.-W. Jeong, *Energy saving potential of liquid desiccant in evaporative-cooling-assisted 100% outdoor air system.* Energy, 2013. **59**: p. 726-736.
11. Kozubal, E., et al., *Desiccant enhanced evaporative air-conditioning (DEVap): evaluation of a new concept in ultra efficient air conditioning*. 2011, National Renewable Energy Lab.(NREL), Golden, CO (United States).
12. Woods, J. and E. Kozubal, *A desiccant-enhanced evaporative air conditioner: Numerical model and experiments.* Energy Conversion and Management, 2013. **65**: p. 208-220.
13. Sohani, A., et al., *A novel approach using predictive models for performance analysis of desiccant enhanced evaporative cooling systems.* Applied Thermal Engineering, 2016. **107**: p. 227-252.
14. Ham, S.-W., S.-J. Lee, and J.-W. Jeong, *Operating energy savings in a liquid desiccant and dew point evaporative cooling-assisted 100% outdoor air system.* Energy and Buildings, 2016. **116**: p. 535-552.
15. Ren, Y., et al., *Experimental study on a cross-flow energy recovered indirect evaporative cooling (ERIEC)-assisted liquid desiccant dehumidifier (LDD) with improved spraying nozzle and surface wetness.* Science and Technology for the Built Environment, 2021. **27**(7): p. 903-916.
16. Yang, L., H. Yan, and J.C. Lam, *Thermal comfort and building energy consumption implications–a review.* Applied energy, 2014. **115**: p. 164-173.

17. Aviv, D., et al., *A fresh (air) look at ventilation for COVID-19: Estimating the global energy savings potential of coupling natural ventilation with novel radiant cooling strategies.* Applied Energy, 2021. **292**: p. 116848.
18. World Health Organization, *Transmission of SARS-CoV-2: implications for infection prevention precautions: scientific brief, 09 July 2020*. 2020, World Health Organization.
19. Chen, Y., H. Yang, and Y. Luo, *Parameter sensitivity analysis and configuration optimization of indirect evaporative cooler (IEC) considering condensation.* Applied Energy, 2017. **194**: p. 440-453.
20. Ren, H., et al., *Optimisation of a renewable cooling and heating system using an integer-based genetic algorithm, response surface method and life cycle analysis.* Energy Conversion and Management, 2021. **230**: p. 113797.
21. Ren, H., et al., *Optimal design and size of a desiccant cooling system with onsite energy generation and thermal storage using a multilayer perceptron neural network and a genetic algorithm.* Energy Conversion and Management, 2019. **180**: p. 598-608.
22. Sohani, A., H. Sayyaadi, and M. Azimi, *Employing static and dynamic optimization approaches on a desiccant-enhanced indirect evaporative cooling system.* Energy Conversion and Management, 2019. **199**: p. 112017.
23. Chen, Y., H. Yang, and Y. Luo, *Parameter Sensitivity Analysis of Indirect Evaporative Cooler (IEC) with Condensation from Primary Air.* Energy Procedia, 2016. **88**: p. 498-504.
24. Woods, J. and E. Kozubal, *On the importance of the heat and mass transfer resistances in internally-cooled liquid desiccant dehumidifiers and regenerators.* International Journal of Heat and Mass Transfer, 2018. **122**: p. 324-340.
25. Liu, J., et al., *Direct contact membrane distillation for liquid desiccant regeneration and fresh water production: Experimental investigation, response surface modeling and optimization.* Applied Thermal Engineering, 2021. **184**: p. 116293.
26. 周立宁, et al., *基于响应曲面法的溶液除湿量双因素交互影响规律研究.* 暖通空调, 2017. **47**(8): p. 122-127.
27. Riangvilaikul, B. and S. Kumar, *An experimental study of a novel dew point evaporative cooling system.* Energy and Buildings, 2010. **42**(5): p. 637-644.
28. W.Y Saman, S.A., *Modelling and performance analysis of a cross-flow type plate heat exchanger for dehumidification/cooling.* Solar Energy, 2001. **70**(4): p. 11.
29. Adam, A., et al., *Numerical investigation of the heat and mass transfer process within a cross-flow indirect evaporative cooling system for hot and humid climates.* Journal of Building Engineering, 2022. **45**: p. 103499.
30. Myers, R.H., D.C. Montgomery, and C.M. Anderson-Cook, *Response surface methodology: process and product optimization using designed experiments*. 2016: John Wiley & Sons.
31. Derringer, G. and R. Suich, *Simultaneous optimization of several response variables.* Journal of quality technology, 1980. **12**(4): p. 214-219.
32. Lam, J.C. and S.C. Hui, *Outdoor design conditions for HVAC system design and energy estimation for buildings in Hong Kong.* Energy and Buildings, 1995. **22**(1): p. 25-43.
33. Zhang, Y., et al., *Energy performance of internally cooled desiccant enhanced evaporative cooling system in Hong Kong.*

Appendix A Significant terms result for analysis of variance (**: p-value<0.01, *: p-value<0.05)

Model	C	Q_{lat}	η_d
A-T_{A1}	**	**	
B-W_{A1}	**	**	*
C-V_{A1}	**	**	**
D-X_S	**	**	*
E-RCD	**	**	**
F-NTU	**	**	**
AB	**	**	
AC	**	**	
AD			
AE	**	**	
AF	**	**	
BC		**	
BD			
BE	**	**	
BF	*	**	
CD	**	**	
CE	**	**	**
CF	**	**	**
DE	**	**	
DF	**	**	**
A^2	**	**	*
B^2			
C^2	**	**	**
D^2	*	**	
E^2		*	**
F^2	**	**	**